International Journal of Mining Science and Technology 28 (2018) 107–113

Contents lists available at ScienceDirect

International Journal of Mining Science and Technology

journal homepage: www.elsevier.com/locate/ijmst

Coal rib response during bench mining: A case study

Morgan M. Sears *, John Rusnak, Mark Van Dyke, Gamal Rashed, Khaled Mohamed, Michael Sloan

Ground Control Branch, NIOSH, Pittsburgh Mining Research Division, Pittsburgh, PA 15236, USA

ARTICLE INFO

Article history:
Received 12 May 2017
Received in revised form 30 June 2017
Accepted 18 August 2017
Available online 23 December 2017

Keywords:
Deep cover
Bench mining
Thick seam
Retreat mining
Rib response
Rib support

ABSTRACT

In 2016, room-and-pillar mining provided nearly 40% of underground coal production in the United States. Over the past decade, rib falls have resulted in 12 fatalities, representing 28% of the ground fall fatalities in U.S. underground coal mines. Nine of these 12 fatalities (75%) have occurred in room-and-pillar mines. The objective of this research is to study the geomechanics of bench room-and-pillar mining and the associated response of high pillar ribs at overburden depths greater than 300 m. This paper provides a definition of the bench technique, the pillar response due to loading, observational data for a case history, a calibrated numerical model of the observed rib response, and application of this calibrated model to a second site.

1. Introduction

Bench mining is an underground mining technique typically applied to room-and-pillar mines where full seam extraction on development presents an unacceptably high risk of injury from high pillar ribs or where the mining equipment is not designed to extract the full seam thickness. To mitigate the increased risk associated with high ribs and slender pillars, a more modest thickness is extracted from the top of the seam on development. This is followed by grading the floor and recovering the bottom of the seam with or without extraction of the pillars during retreat mining.

A mine located in Eastern Kentucky extracts two seams at depths ranging from outcrop to over 600 m. In some areas of the mine, Seam A and Seam B are close enough together to be mined simultaneously. Seam A (top) is mined on development 2–3 m high for the entire length of the panel. On retreat, as each pillar is extracted, the continuous miner is ramped down into the floor (Seam B), two pairs of mobile roof support (MRS) units are set, and the pillars are extracted at the full mining height of 4+ m. During the pillar recovery process, the floor is extracted in each entry, from a ramp initiated outby the retreat line, sequentially just prior to extracting the lifts from the pillars (Fig. 1).

Current rib support practices at the mine include the use of 1.5-m-long, 19-mm-diameter, grade 60, fully grouted tensioned rebar bolts installed with 20 cm × 40 cm steel bearing plates. Typically, one row of bolts is installed if the mining height is less than 3 m, two rows are installed if the mining height is from 3 to 4.5 m, and three rows are installed if the mining height is greater than 4.5 m. Row spacing for the top row is 1.2 m, while spacing for the second or mid-pillar row can be increased to 2.4 m if the bolts are anchored in the rock parting. Typically, the third row is installed just prior to retreat mining at a maximum 2.4-m spacing. During retreat, loose ribs are cut down and re-supported as necessary, which can include the installation of extended length (2.4-m) rib bolts if required [1].

2. Rib model development

Numerical modeling is a useful tool to help explain the stress distribution and extent of rib fracturing in coal pillars. In order to investigate the stress distribution and development of rib fractures at this mine, the finite difference software FLAC3D was used [2]. Fig. 2 shows the geologic column that was simplified into four coal layers and two stone layers for use in the FLAC3D model. The FLAC3D model for the first case history site is a three-dimensional model for a single pillar, 18 m wide and 30 m long, rib to rib. Three pillar configurations were considered in the initial model to better elucidate how each behaves during loading. The pillar models were monotonically loaded to failure. The short pillar represents development mining Seam A, which is labeled "Advance" in Fig. 2.

* Corresponding author.
E-mail address: msears@cdc.gov (M.M. Sears).

https://doi.org/10.1016/j.ijmst.2017.12.010
2095-2686/

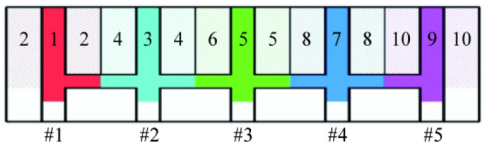

Fig. 1. Sequential floor removal in each entry prior to retreat mining.

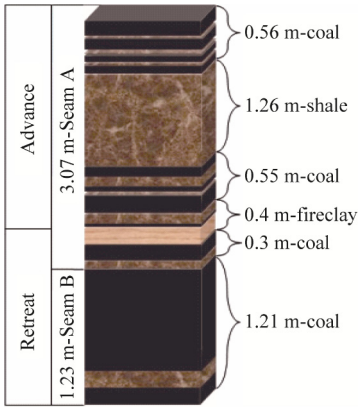

Fig. 2. Typical stratigraphic column simplified for the FLAC3D model.

The slender pillar represents mining the full seam height of both seams at the full extraction thickness of 4+ m. Although this configuration never occurs in the field, it was chosen to be modeled solely for comparison purposes. Finally, the third configuration modeled the benched pillar as close to the proposed design as possible with one entry ramped down into Seam B right before pillar extraction would begin (see Fig. 3). No rib supports were simulated in these models, and the benched model is capable of simulating retreat mining right to left or left to right simply by changing the orientation of the cleat system.

The bottom boundary of the model is constrained in the z-direction. Roller supports are assumed in the x-direction at both the left and right entries. Roller supports are also assumed in the *y*-direction at the inby and outby crosscuts. The element size in the pillar is about 25 cm in both the *x* and *y* directions. The smallest and largest element sizes in the z-direction of the modeled pillars are 15 and 30 cm, respectively.

Tables 1 and 2 show the rock and coal properties in the FLAC3D model. The field observations at Site 1 and Site 2 show that the immediate roof and floor strata were intact. Therefore, the roof and floor strata were modeled as elastic material models. Field inspection showed that a soft band located at the top of Seam A is extremely influential in the mode of failure and extent of rib deterioration. Therefore, a relatively soft pillar/roof interface was assumed. The Coulomb friction model was assumed for the Seam A/roof rock interface, and the friction angle and the cohesion of the interface were 10° and 100 kPa, respectively. The normal and shear stiffness of the interface between pillar and roof were assumed to be 1.00 and 0.50 MPa/m, respectively.

Recently, National Institute for Occupational Safety and Health (NIOSH) researchers Mohamed et al. developed a coal material

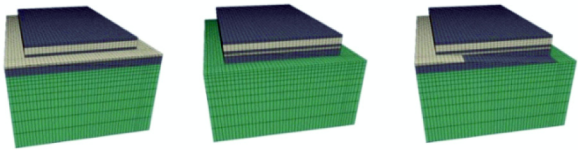

(a) Short pillar (b) Slender pillar (c) Benched pillar

Fig. 3. Pillar layouts.

Table 1
Input parameters for coal material.

	Coal seam	A	B
Elastic property	Modulus (GPa)	2.760	4.550
	Poisson's ratio	0.250	
Strength parameter	σ_{ci} (MPa)	21.000	35.000
	m	3.510*	
	s	0.065*	
	a = constant	0.500	
	$\sigma_{cr=3.085} \times (D, mm)^{-1.241}$ (MPa)	1.380*	
	$\sigma_c = \sigma_{ci} \times s^a$ (MPa)	5.350*	8.920*
Degradation parameter	$n_{d=0.144} \times \ln(D, mm) - 0.568$	0.327*	
	$\Upsilon^p_{crit=0.1} \times (D, mm)^{-0.44}$	0.154*	
Ubiquitous joint friction angle (°)		25.000**	
Fracture plastic shear strain		0.030**	
Fracture plastic tension strain		0.003**	

* Means the strength parameters for coal-mass size (D) of 500 mm.
** Refers to calibrated parameters.

Table 2
Input parameters for stone material.

Rock strata		Roof/floor	Shale	Fireclay
Elastic property	Modulus (MPa)	20.000	10.000	8.000
	Poisson's ratio		0.250	
Strength parameter	σ_{ci} (MPa)	Elastic	48.000	43.000
	m		6.859	2.341
	s		0.189	
	a		0.500	
	σ_{cr} (MPa)		2.600	
	$\sigma_c = \sigma_{ci} \times s^a$ (MPa)		20.870	18.700
Degradation parameter	n_d		0.200	
	Υ^p_{crit}		0.123	
Ubiquitous joint friction angle, degree			25.000	
Fracture plastic shear strain			0.020	
Fracture plastic tension strain			0.002	

model [3,4]. In this model, the peak strength of the coal is evaluated by the generalized Hoek–Brown failure criterion. The residual stiffness and strength are evaluated by the Fang and Harrison local degradation model [5]. The dilation of the coal material is defined by the Alejano and Alonso peak-dilation model [6].

Mohamed, Tulu, and Murphy indicated that the Mohr–Coulomb constitutive model provides a method for describing the dilation behavior of rocks, and it is available in the majority of numerical codes [4]. Therefore, in this model, the equivalent Mohr–Coulomb model parameters, derived from the Hoek–Brown criterion, are used. This model simulates the peak and post-peak behaviors of the coal material by using the strain softening, ubiquitous joint model available in FLAC3D. The coal material model has been calibrated to field cases and fully implemented in the FLAC3D program as a user-defined constitutive model.

Input parameters used for Seam A and Seam B in this paper are summarized in Table 1. In Table 1, σ_{ci} is the intact unconfined compressive strength of the coal, and m, s, and a are the scaled peak strength parameters of the coal as used in the Hoek–Brown failure criterion. The σ_{ci} is estimated from the coal brightness profiles of the respective seams with Seam A having a bright and dull banded composition, and Seam B being predominantly dull coal. σ_c is the peak, and σ_{cr} is the residual of the field-scale unconfined compressive strength. n_d is a scaled coal degradation parameter. This degradation parameter is used to reduce the strength and stiffness of the coal from peak values to residual values in the coal model [3,4]. Υ^p_{crit} is the scaled critical plastic shear strain. Coal material

fracturing is simulated by adding implicit cohesion-less ubiquitous joints within the material. Fractures are initiated in those elements that have plastic strains (shear and tension) equal to or greater than the "fracture plastic strain" parameters detailed in Table 1. A modified version of this coal model was used to simulate the fractures developed in the stone units (shale and fireclay) in the pillar ribs. The input parameters used for shale and fireclay in this paper are summarized in Table 2.

3. Benched pillar behavior

In order to explore the differences in the three pillar layouts (Fig. 3), each model was loaded progressively from the top well into the post-failure range. As the load increased, the average axial displacement was monitored across the top of the pillar, as shown in Fig. 4. Axial displacement was chosen rather than strain due to the differing mining heights for the benched pillar scenario. As expected, all three pillars exhibit strain softening behavior with the stress displacement relationship of the benched pillar falling between that of the short pillar and the slender pillar. However, this model shows that the peak strength of the benched pillar is only about 6% stronger than that of the slender pillar.

For rib control purposes, the lateral displacement of the pillar is of greater importance because that directly translates to the movement mine personnel is attempting to control. Lateral displacement for each of the three pillar models was monitored at the center of the pillar perpendicular to the entry orientation. To compare the three pillar configurations, points near the top (90% of height), middle, and bottom (10% of height) of the rib were plotted for lateral displacement as load was applied to the top of the pillar (Fig. 5). As expected, the right rib, which has been benched, closely matches the load-displacement curve modeled for the slender pillar configuration. However, the left rib of the benched pillar does not match the displacement of the short pillar in this model. Especially at the top of the rib, where soft pillar-to-roof contact was assumed, the predicted lateral rib displacement for the left rib of the benched pillar was much greater that of the short pillar. This implies that, based on this model, the load-displacement characteristics of the benched pillar, for both vertical and horizontal displacements, more closely match those of the slender pillar than those of the short pillar.

4. Model calibration

Observations and measurements taken during active retreat mining in the current panel (site 1) were used as the basis for the calibration of the pillar model that was discussed in the previous section. This site provided unique opportunities for observations of both short pillar (development) and benched pillar configurations under both development and abutment loads. The pillar of interest at Site 1 is located on the pillar line of the next pillar row to be extracted. The overburden depth at the surveyed site was about 425 m. The pillars at Site 1 were 18 m wide by 30 m long, rib to rib. The face cleats of both Seam A and Seam B are oriented at an angle of 60° counter-clockwise from the entry direction. Fig. 6 shows the location of the observed pillar (1), the gob area in red hatch, and the benched area in green hatch. Rehabilitation of the rib support in this area was already completed at the time of observation. Fig. 6 depicts the current mining at the time of observation, and the green hatch represents the approximate state of benching in the area that was encountered.

To provide a reasonable estimate of the loads applied to the pillar during retreat mining, the LaModel program was used [7,8]. First, the 18 m × 30 m pillars were discretized using 1.5-m elements. A mining height of 2.4 m was chosen to simulate pillars that

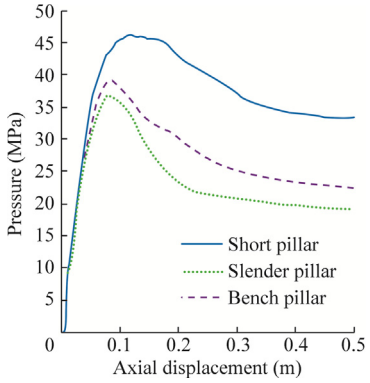

Fig. 4. Applied pressure versus axial displacement.

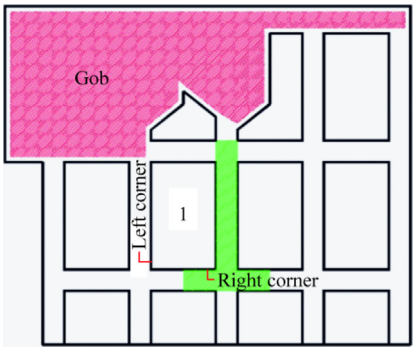

Fig. 6. Observed pillar at site 1 with the benched area hatched in green.

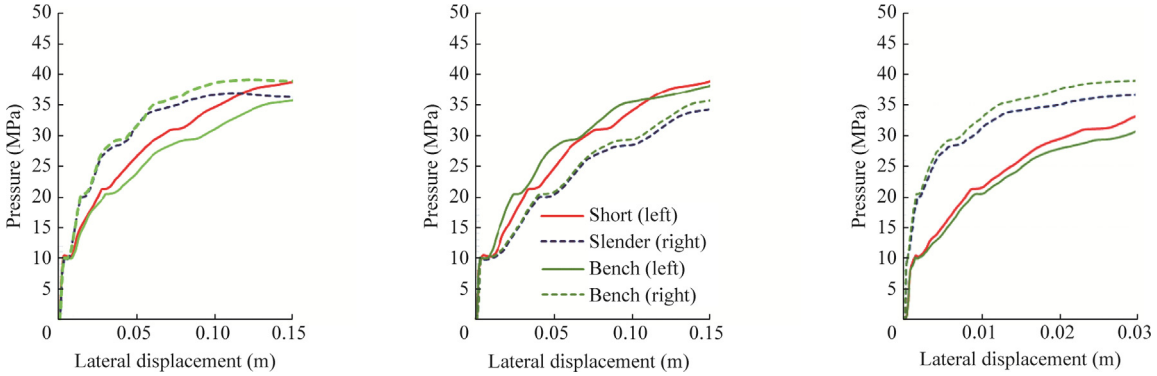

Fig. 5. Applied pressure versus lateral displacement.

were not yet benched. The pillar strength was then calculated assuming an in-situ coal strength of 6.2 MPa using the Mark-Bieniawski formula [9]. The deep cover LaModel calibration suggested by Heasley et al. was then used to calibrate the lamination thickness of the rock mass, matching the empirically suggested abutment extent where 90% of the abutment load occurs within a distance of $5\sqrt{(H)}$ [10,11]. Finally, the final gob modulus was calculated to provide an average gob loading, matching the empirically suggested 21° abutment angle. The abutment stresses calculated by the LaModel analysis were then used to determine the appropriate amount of loading in the vertical direction for application to the benched pillar in the FLAC3D model. The FLAC3D models were then solved in four steps: (1) applying the pre-mining in-situ stresses, (2) excavating the entries and crosscuts for Seam A development, (3) excavating the entries and crosscuts for Seam B development, and (4) applying the abutment load, obtained from LaModel, gradually at the top of the model.

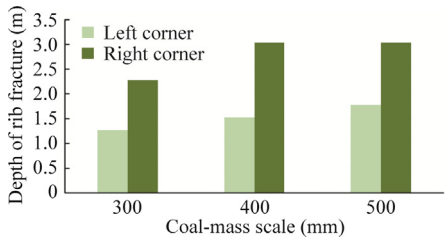

Fig. 7. Depth of rib fracture (DRF) versus coal-mass scale.

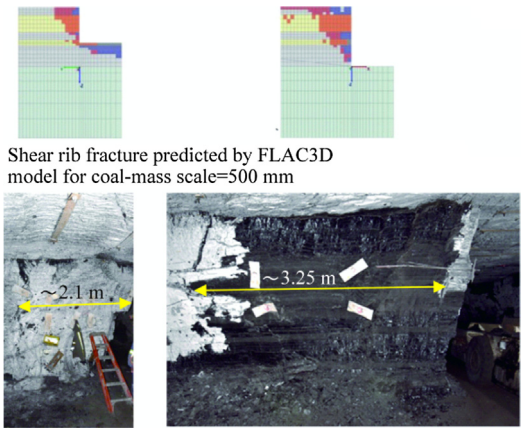

Fig. 8. Model versus field observations under abutment loading conditions at Site 1.

The extent of rib damage is largely controlled by a parameter *D* called the "coal-mass scale," as shown in Table 1. Essentially, this parameter is analogous to the specimen size with smaller values representing a strength/stiffness closer to lab scale and larger values representing a strength/stiffness closer to pillar scale. Consequently, a coal material with a smaller coal-mass scale is stronger and stiffer than that with a larger coal-mass scale. Previous coal model calibrations showed the coal-mass scale could range from 300 to 500 mm [3,12]. A range of coal-mass scales including 300, 400, and 500 mm, were applied to the model. The depth of rib fracture for each coal-mass scale is predicted at the right and left corners of Site 1, as shown in Fig. 7. Ultimately, a coal-mass scale of 500 mm was selected because it matched the observed rib conditions on the left and right rib corner based on the benched pillar model (see Fig. 8). It should be noted that the model does not differentiate between the directions in which the fracture is occurring. This means that it does not differentiate between fractures that would cause coal to be sloughed into the entry vs. the crosscut.

5. Model results

5.1. Site 1

The results from the calibrated FLAC3D model are presented using two graphical approaches. First, the rib displacement contours and the rib displacement profile at the right corner of the outby crosscut are shown in Fig. 9. The rib displacement contour plot shows that, for Site 1, more displacement is occurring in the crosscut than either the benched or unbenched entry because the face cleat orientation of the coal seams is an angle of about 30° with respect to the crosscut orientation. The rib displacement is shown at the same corner location that the depth of fracture was measured from the model during the calibration phase. This plot shows that a maximum displacement occurs near the roof line of just under 0.3 m. It was noted during observations that there was little to no observable roof sag in the area, and, although the floor was soft in places, there was no major observable floor heave. Contacts at the roof-coal interface were very smooth and often slickensided while the floor-coal contact was much stronger. To the observer, it appears that the rib compresses and displaces outward toward the opening. Also, the contact at the floor-coal interface prevents movement at the base of the pillar, and the slick nature of the interface with the roof allows the top of the rib to slip outward. This results in substantially more rib displacement observed at the roof line than that observed at the floor, as shown

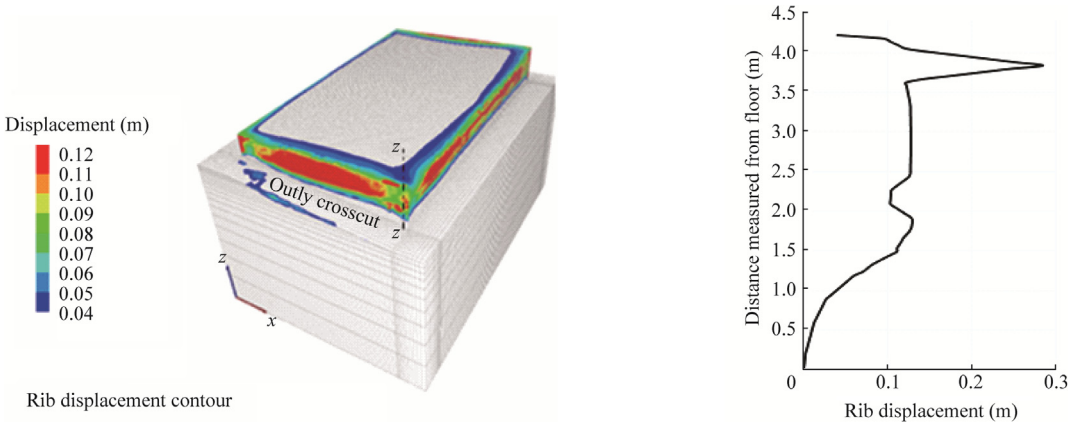

Fig. 9. Rib displacement during abutment loading for Site 1.

in Fig. 9. This correlates well to the observed conditions shown for the right corner in Fig. 8.

The next graphical representation plots elements within the model that have yielded or fractured. As with most numerical models, the yield of an element will occur when the stress level in the element surpasses its peak strength on the stress-strain envelope. The element could yield under tension or shear stress. This model differentiates between rib yielding and fracture. Rib fracture is simulated by imposing implicit cohesion-less ubiquitous joints. In this model, fracture of an element is assumed to occur at 3% plastic strain for shear (red fringes) and 0.3% plastic strain for tension (blue fringes), as shown in Fig. 10. The element fracture is a unique fracture in the developed coal/stone material models and was calibrated to provide the best match between the observed rib fractures and the model results. From Fig. 10, it is clear that the depth of rib yielding (DRY) is much greater than the depth of rib fracturing (DRF). This occurs regardless of the failure mode being either tension or shear. This also implies that the objective of rib support is not to attempt to control the yielding of the rib, but rather to try to control the fractured portion of the rib.

Fig. 11 depicts a bar chart of DRY and DRF under shear for the left (short) and right (benched) ribs of the pillar at section *x*–*x* (see Fig. 10) during development, benching, and under the abutment loading during retreat mining. For the left (short) entry, the DRF changes very little as benching progresses in the adjacent entry (in Seam B development) and as the abutment loading is added to the model. However, for the right (benched) entry, the depth of fracturing increases significantly upon benching but does not increase significantly as the abutment load is applied to the pillar. This appears to be confirmed by observations at the time of retreat mining. Specifically, prior to retreat mining during the floor grading process, significant rib sloughage was observed, loose ribs were cut down with the continuous miner, and additional support was installed prior to mining in that entry. During retreat mining, however, addition rib sloughage was not observed at Site 1. The DRY, on the other hand, increases throughout the benching and loading cycle over the life of the pillar.

5.2. Site 2

Site 2, the next panel to be retreat mined, was visited during development at the same time Site 1 was visited. Development at Site 2 was proceeding at the proposed 2.4-m mining height, extracting only Seam A. However, this site was about 120 m deeper (550 m) than site 1. The pillars at Site 2 were 21 m wide by 30 m long—3 m wider than the pillars at Site 1. Also, the face cleat of Seam A at Site 2 was found to be parallel to the entry orientation. Therefore, to better understand the conditions that might be encountered at Site 2 during retreat mining, the model that was calibrated for Site 1 was modified to include the new overburden stresses and to account for the change in face cleat orientation.

Under Seam A development loading conditions, very little damage of the recently exposed rib was observed at Site 2 (see Fig. 12). Using the calibrated coal model developed for Site 1, the modeled rib response for Seam A development closely matches what was observed in the field with the conditions shown in Fig. 12. The

Fig. 12. Observed rib conditions at Site 2.

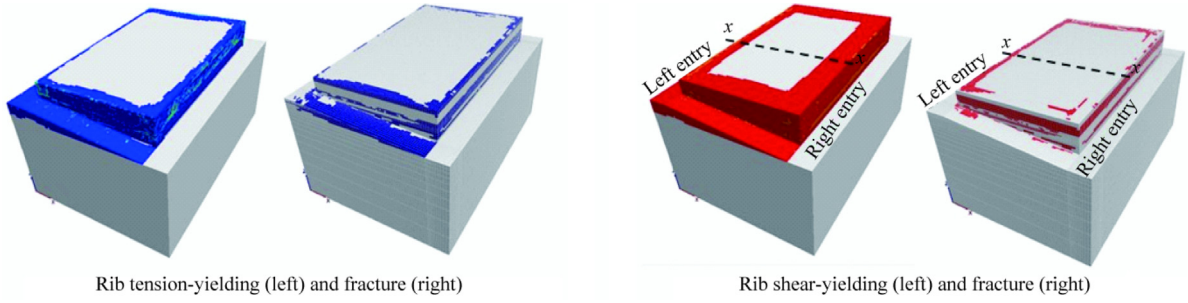

Fig. 10. Rib yielding and fracture during abutment loading at Site 1.

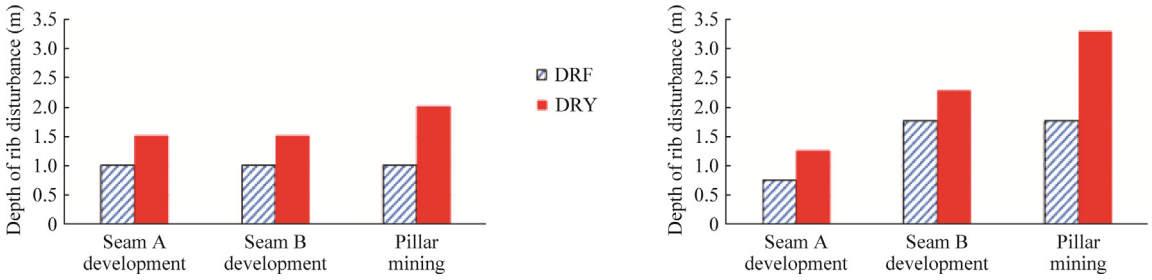

Fig. 11. Depth of rib fracture (DRF) and yielding (DRY) along a cross section at the pillar center.

modeled rib displacement for Seam A and Seam B development is shown in Fig. 13. Looking at the rib displacement contours on the left, one sees more displacement occurring in the entry for both Seam A and B mining at Site 2. This is due to the orientation of the face cleat being parallel to the entry. Comparing a rib corner in a manner similar to Site 1 indicates the same shape of the rib displacement profile, albeit with a much smaller displacement of 0.04 m for Seam A development and about 0.08 m for Seam B development at Site 2.

Contour plots of rib yielding and fracture for site 2 during Seam A development are shown in Fig. 14. Rib yielding and fractures in tension are illustrated by blue fringes, and rib yielding and fracture in shear are illustrated by red fringes. Similarly to field observations, slight rib fractures were predicted by the FLAC3D model. Once again, the DRY far exceeds the depth of the DRF observed in the rib regardless of the failure mode. Due to the face cleat orientation, the depth of fracture is deeper when parallel to the face cleat, in this case along the entry.

Fig. 15 depicts a bar chart of DRY and DRF under shear for the left (short) and right (benched) ribs of the pillar at section *x*–*x* (see Fig. 14) during development, benching, and under the abutment loading during retreat mining. As expected, the depth of yield increases throughout the loading cycle. In contrast to the model behavior for Site 1, the depth of rib fracture also increases after benching as the abutment load is applied to the pillar.

6. Summary

This paper has defined, described, modeled, and analyzed room-and-pillar bench mining with full pillar extraction. Based on the initial analysis of the behavior of the three pillar configurations—short, slender, and benched—the FLAC3D model suggests that a benched pillar behaves more like the slender pillar than the short variant. This applies to both vertical and axial displacement over the course of loading.

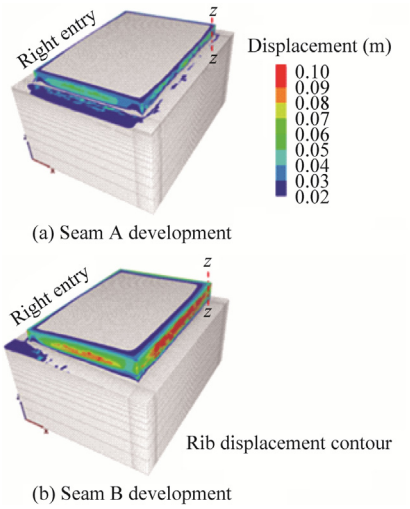

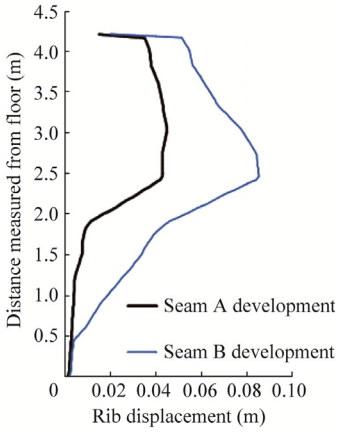

Fig. 13. Rib displacement contours and profile at the right corner for Site 2.

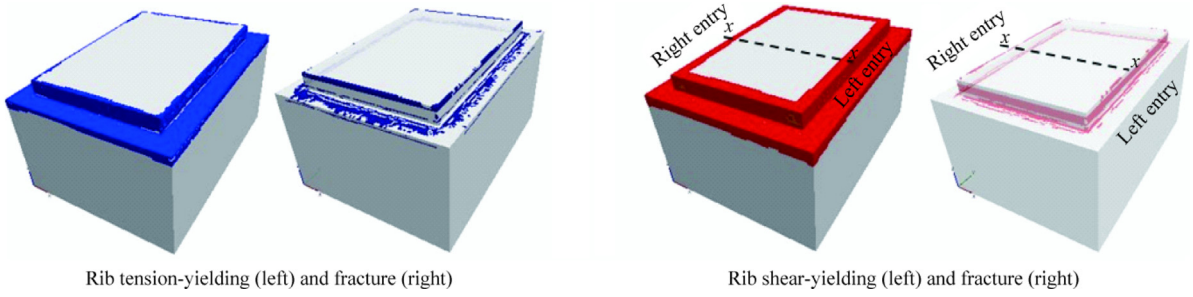

Fig. 14. Rib yielding and fracture during Seam A development loading at Site 2.

Fig. 15. Depth of rib fracture (DRF) and yielding (DRY) along a cross section at the pillar center at Site 2.

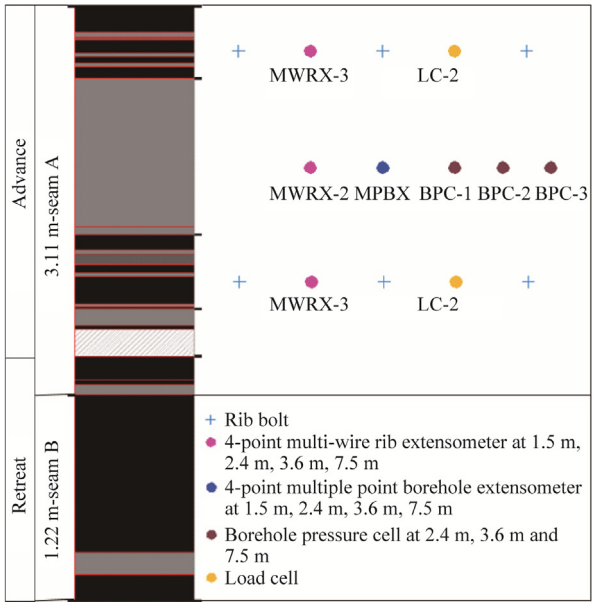

Fig. 16. Proposed rib monitoring plan.

The FLAC3D model was then calibrated to match the conditions at site 1 where development, benching, and abutment loading were observed. Abutment loads were estimated using the LaModel program and applied to the FLAC3D model to simulate the effects of the abutment loading during retreat mining. Calibration of the FLAC3D model to the observed field conditions required adjustment of the coal-mass scale, a critical input parameter controlling the amount of disturbance and, consequently, fracturing of the pillar. A coal-mass scale of 500 mm seemed to most accurately represent the observed conditions.

Inherent to the definition, the depth of rib yielding exceeds the depth of rib fracture during all phases of loading. For Site 1, the model suggests that, along the cross section at the centerline of the pillar, perpendicular to the entry, the DRF was about 1.8 and 1.0 m for the benched and unbenched entries, respectively. The predicted DRY was 2.0 and 3.3 m for the benched and unbenched entries, respectively. Attempting to control the depth of rib yielding using a support system is impractical. Instead, the focus for rib support should be applied to controlling the rib during and after fracture formation.

Finally, the calibrated FLAC3D model was applied to a second case, Site 2. Observations at Site 2 were made during development mining of the Seam A. Minimal rib damage was observed in this area, which closely matches the modeling results of 0.8 m DRF and is less than 0.05 m of rib displacement for that loading condition. The FLAC3D model for Site 2 was then used to predict the amount of rib displacement and fracturing during subsequent benching and pillar extraction. The depth of rib fracturing is predicted to increase when the seam is benched, followed by a second increase during retreat mining. The final predicted fracture depth was modeled to be 3.0 and 2.3 m for the benched and unbenched entry, respectively.

This research explores rib control and modeling in a retreat bench mining scenario that is different than conventional retreat mining. Additionally, a new rib model was developed by NIOSH researchers, incorporating the face cleat orientation, thereby providing a better understanding of rib deformation that occurs underground in a complex loading scenario. The results of this research not only provide a better understanding of fracture development in benched coal ribs but also provide needed groundwork for developing better 3D models for further rib control research.

7. Proposed instrumentation

Suggestions for future research include additional observation at Site 2 during retreat mining, as well as a proposed instrumentation site in a future panel. Based on the findings of this study, the rib monitoring plan in Fig. 16 is proposed.

Due to the timing involved with benching followed by pillar extraction, there is not enough time to install any instrumentation into Seam B. Instead, a series of three multi-wire rib extensometers (MWRX) near the top, middle, and bottom of Seam A should be installed to measure rib displacement at these horizons. Additionally, a multi-point borehole extensometer should be installed to verify the measurements of the MWRX. Three borehole pressure cells will be installed to measure vertical pressure change in the rib as mining progresses. Finally, two load cells should be installed to measure load on the installed rib bolts. The results of this measurement can be used for better understanding of the rib behavior and for additional calibration and verification of the models presented in this paper.

Disclaimer

The findings and conclusions in this paper are those of the authors and do not necessarily represent the views of the National Institute for Occupational Safety and Health (NIOSH). Mention of any company or product does not constitute endorsement by NIOSH.

References

[1] Mohamed KM, Murphy MM, Lawson HE, Klemetti T. Analysis of the current rib support practices and techniques in U.S. coal mines. Int J Min Sci Technol 2016;26(1):77–87.
[2] Itasca. FLAC3D. Minneapolis, MN: Itasca Consulting Group, Inc. http://www.itascacg.com/software/FLAC3D; 2015.
[3] Mohamed KM, Tulu IB, Klemetti T. Numerical simulation of deformation and failure process of coal-mass. In: Proceedings of the 49th US Rock Mechanics/Geomechanics Symposium. Alexandria, VA: American Rock Mechanics Association; 2015.
[4] Mohamed K, Tulu B, Murphy M. Numerical model calibration for simulating coal ribs. In: Proceedings of the 35th International Conference on Ground Control in Mining. Morgantown, WV: West Virginia University; 2016. p. 289–298.
[5] Fang Z, Harrison JP. Development of a local degradation approach to the modeling of brittle fracture of heterogeneous rocks. Int J Rock Mech Min Sci 2002;39(4):443–57.
[6] Alejano LR, Alonso E. Considerations of the dilatancy angle in rocks and rock masses. Int J Rock Mech Min Sci 2005;42(4):481–507.
[7] Heasley KA. Numerical modeling of coal mines with a laminated displacement-discontinuity code. Doctoral Thesis. Golden, Colorado: Colorado School of Mines; 1998. p. 374.
[8] Klemetti TM, Sears MM, Tulu IB. Design concerns of room and pillar retreat panels. Int J Min Sci Technol 2017;27(1):29–35.
[9] Mark C. Empirical methods for coal pillar design. In: Proceedings of the 2nd International Workshop on Coal Pillar Mechanics and Design Workshop. Morgantown, WV: West Virginia University; 1999. p. 145–54.
[10] Heasley KA, Sears MM, Tulu IB, Calderon-Artega C, Jimison L. Calibrating the LaModel Program for Deep Cover Pillar Retreat Coal Mining. In: Proceedings of the 3rd International Workshop on Coal Pillar Mechanics and Design Workshop. Morgantown, WV: West Virginia University; 2010. p. 12.
[11] Mark C, Chase FE. Analysis of retreat mining pillar stability (ARMPS). In: Mark C, Tuchman RJ, editors. Proceedings of the New Technology for Ground Control in Retreat Mining. Pittsburgh, PA: National Institute for Occupational Safety and Health; 1997. p. 17–34.
[12] Zhang P, Mohamed K, Trackemas J. Coal rib failure and support in longwall gate entries. Unpublished paper at the 51st US Rock Mechanics/Geomechanics Symposium. San Francisco; CA; 2017 June 25–28.